Application of infrared thermography technique to the thermal assessment of multiple thermal bridges and windows

Małgorzata O'Grady [a], Agnieszka A. Lechowska [b], Annette M. Harte [a],*

[a] College of Engineering and Informatics & Ryan Institute, National University of Ireland Galway, Galway, Ireland
[b] Department of Environmental Engineering, Cracow University of Technology, Cracow, Poland

ARTICLE INFO

ABSTRACT

A major contribution to the global trend in reducing energy consumption can be made by improving the thermal performance of buildings. Minimization of heat loss via the building envelope is key to maximizing building energy efficiency. The building envelope contains different types of thermal bridging that must be accounted for while assessing the overall building envelope thermal performance. Multiple thermal bridges commonly occur and the distance between them determines the degree to which they interact thermally. To avoid overestimation of the linear thermal transmittance, it is important to account for interaction effects. Complex multiple thermal bridging occurs in window systems. The thermal performance of windows depends not only on the window performance itself but also on its installation into the wall. This study demonstrates an application of the quantitative infrared thermography technique to evaluate the heat lost via multiple thermal bridging. It is shown that using this methodology, the heat loss via multiple thermal bridges can be easily estimated in an existing building envelope, without any knowledge of its internal structure or material properties. For windows, it is demonstrated that jointly assessing the additional heat loss through the window and due to the installation of the window into the wall is a practical way to determine the actual heat loss caused by the presence of a window. A window thermal transmittance or M-value is introduced to quantify the total additional heat loss through the building element due to the presence of the window. The methodology was validated against experimental measurements taken on different specimens in a hot box device. Results from the thermographic analysis also co-related well with results from finite element heat transfer and computational fluid dynamics simulations.

1. Introduction

Buildings are associated with approximately one-third of global primary energy consumption and one-third of total energy-related greenhouse gas emissions [1]. In order to limit energy consumption related to buildings at a European level, the European Union Directive 2010/31/EU on Energy Performance of Buildings (EPBD 2010) [2] defined minimum targets for EU Member States in relation to national building regulations. Consequently, building regulations within EU countries became stricter on building energy performance. Evaluation of EPBD 2010 [3] revealed that these changes have had a particularly positive impact on energy performance improvement of newly constructed buildings. Nevertheless, a large portion of the existing buildings still needs deep retrofitting to meet the minimum thermal performance requirements. This pro-

vides opportunities for significant energy savings but is, at the same time, a major challenge due to the large number of buildings involved.

When considering building energy efficiency, several factors should be taken into account; however, the role of the building envelope in providing a barrier between the indoor and outdoor environments cannot be underestimated. The thermal standard of a building envelope is one of the major factors to be considered in ensuring that a building is energy efficient [4]. The building envelope consists of plain components of uniform thermal resistance together with regions of thermal bridging. Because a thermal bridge represents part of a building envelope with higher thermal conductivity or different geometry, it is associated with significantly higher heat losses than the plain component surrounding the thermal bridge. It is crucial to account for this additional heat loss while assessing the building envelope thermal performance. Two types of thermal bridging can be distinguished: a point thermal bridge, which appears at the connection of three building components and a linear thermal bridge, characterized by a uni-

Nomenclature

A	area of the specimen, m^2
α	thermal diffusivity, m^2/s
β	expansion coefficient, $1/K$
ε	surface emissivity, dimensionless
Φ	heat power, W
g	acceleration due to gravity, m/s^2
h	heat transfer coefficient, $W/(m^2K)$
H	height, m
ITT	Infrared thermography technique
l	length, m
k	thermal conductivity of air, $W/(m^2K)$
ν	kinematic viscosity, m^2/s
Nu	Nusselt number, dimensionless
M	window thermal transmittance, W/K
$\dot{m}$	mass flow rate, kg/s
Pr	Prandtl number, dimensionless
q	heat flow rate per unit height, W/m
$\dot{q}$	surface heat flux, W/m^2
$\dot{Q}$	heat flow rate, W
Ra	Rayleigh number
RD	relative percentage deviation, %
σ	Stefan-Boltzmann constant, $W/(m^2K^4)$
T	temperature, °C
u	uncertainty, the unit depends on the measurement
w	air velocity, m/s
ρ	density, kg/m^3
Φ	heat power, W
Ψ	linear thermal transmittance, $W/(mK)$

Subscripts

c	convective
ch	characteristic
b	baffle
e	cold side, external conditions
$edge$	edge zone between the specimen and the surrounding panel
i	warm side, indoor conditions
in	input to the hot box
min	minimum
n	environmental
$plain$	component without thermal bridge
r	radiative
s	surface
$S1$	sensor 1
$S2$	sensor 2
sp	specimen
sur	surrounding
TB	thermal bridge
tot	total
u	uniform
x	pixel

form cross-section along one of the three orthogonal axes [5]. The heat loss related to linear thermal bridges may be described by the linear thermal transmittance (Ψ-value). According to standard ISO 14683 [5], it expresses the heat flow rate in a steady state per unit length and per degree of difference in the indoor and outdoor air temperatures on each side of a thermal bridge. There are several ways of obtaining the linear thermal transmittance. The simplified way is to use default values given in this standard. However, they only apply to standard building details and their typical accuracy varies between 0% and 50%. A more sophisticated and widely-used approach to evaluate the Ψ-value is through numerical calculation.

Detailed instructions about how a Ψ-value can be derived from a numerical model are given in EN ISO 10211 [6]. To build a model, the construction of the thermal bridge and of the plain components must be known. Therefore, this approach is suitable at the design stage.

The numerical and analytical approaches have been widely used by researchers to predict thermal bridging performance. Capozzoli et al. [7] used finite element (FE) modeling to carry out a sensitivity analysis of the factors influencing heat flow through thirty six common thermal bridges in masonry structures. For cases where internal or external insulation continues over the thermal bridge, they identified the thickness of the insulation layer as the most significant variable that influences the Ψ-value. In cases with non-continuous insulation, variables such as the thermal conductivity of the masonry and floor, roof and wall thickness are also important. However, masonry thermal conductivity has a greater impact on the Ψ-value than its thickness. Viot et al. [8] suggested that the most accurate way of thermal bridging heat loss evaluation is using an unsteady 3D heat transfer model. Hassid developed an analytical approach to evaluate thermal bridging heat loss located in both, homogeneous [9] and multilayer walls [10] that showed good agreement with numerical results. Using this approach, the effect of different parameters such as thermal bridge and plain component thicknesses and their conductivities can be also assessed.

Considering the thermal bridges located in an existing building, their structure is very often unknown. In this case, a measurement method must be used to evaluate their heat loss. The Irish Building Regulations [11] allow determination of the Ψ-value from measurement. However, there is no standardized measurement method. To experimentally measure heat loss via thermal bridges some researchers [12–14] have used heat flow meters (HFMs) that were placed on the thermal bridge and at the significant distance away from the thermal bridge. The qualitative infrared thermography technique (ITT) was used as a supplementary technique to locate the thermal bridge and correctly position HFMs.

A quantitative ITT approach was used by Heinrich and Dahlem [15] to find the distribution of the indoor surface temperature of a lightweight wall containing an I-beam, and this was then compared with numerical simulations. They reported that the thermal bridge zone of influence in the numerical model was smaller than that recorded by the ITT. Wróbel and Kisielewicz [16] used a quantitative ITT to define the lowest surface temperature on the thermal bridge. To extend evaluation to other environmental conditions, they used numerical simulation. Fox et al. [17] compared the effectiveness of indoor and outdoor qualitative thermographic surveys in building defect identification. They found that, in almost 60% of all tested dwellings, the defects could be detected from both sides, but the indoor ITT presented the defects more clearly. In 40% of cases, the defects were located using the indoor thermography and they were not visible while taking the external survey. In only 2% of dwellings, detection of anomalies was possible externally and not internally.

Benkő [18] was one of the first researchers to assess the heat loss associated with thermal bridging by means of the outdoor quantitative ITT. On an IR image of a building wall, two surface temperatures were identified: one on the thermal bridge and the other on the plain part of the building envelope not affected by the thermal bridge. Based on these temperatures, Benkő defined an energy saving factor that expressed the proportion of the heat losses of a building component including and excluding thermal bridging influence. Similarly, Asdrubali et al. [19] described the heat loss via thermal bridging as a factor showing how the heat loss through a building component increases due to the presence of the thermal bridge, using the indoor ITT. Their approach is more precise than the Benkő method as it accounts for the temperature in each pixel. Asdrubali et al. [19] validated the methodology under labora-

tory conditions on a thermal bridge between a window frame and glazing. To fully quantify the thermal bridging heat loss, they multiplied the factor by the U-value of the plain component measured by a heat flow meter (HFM). Their methodology has been validated on a test room by Bianchi et al. [20]. O'Grady et al. [21] expanded the last approach and introduced a methodology that allows quantification of the thermal bridge heat flow rate q_{TB} and the linear thermal transmittance Ψ-value by means of the ITT alone. Their methodology was adapted for outdoor ITT where weather conditions, especially wind, significantly influence the building surface temperatures [22].

The literature shows that various approaches to evaluate the heat loss through a single linear thermal bridge have been developed. In the building envelope, thermal bridges rarely occur in isolation and multiple thermal bridges must often be accounted for in assessment of the thermal performance of the building envelope. The distance between the thermal bridges determinates the degree of interaction between them. If they are located close to each other, the heat flow rate through one thermal bridge affects the heat flow rate of the other. Ward and Sanders [23] give some guidelines of how to account for this interaction in numerical modeling. According to Ward and Sanders [23], two adjacent thermal bridges that are located less than the thickness of the building component apart, should be included in the same numerical model. This prevents an overestimation of their Ψ-values. Thermal bridges located at a greater distance apart are assumed not to interact and independent numerical models can be created.

All buildings have installed windows, which may be considered as complex multiple thermal bridging systems. The total heat loss through the window consists of heat losses via window glazing, window frame and the connection between them. According to ISO 10077-1 [24] all these heat losses, expressed by U-value of the frame, U-value of glazing and Ψ-value of the window frame and glazing connection are to be included in the window U-value. This U-value is specified for a range of windows available on the market by numerical evaluation, according to ISO 10077-1 [24] or hot box method in accordance with EN ISO 12567-1 [25].

Once the window is fixed into the building wall, additional thermal bridging, as a result of junctions between the window and the wall, occurs. According to BRE Scotland [26], this Ψ-value around windows is to be determined numerically. In the model, only the building wall is included, and adiabatic boundary conditions are assumed where the window frame connects to the wall. The Ψ-value around windows calculated this way depends only on the dimensions of the frame and on its location in the jamb. A more rigorous approach to the installation Ψ-value is presented by the Passive House Institute [27]. According to their procedure, this heat loss is also evaluated numerically; however, their model includes the window and therefore accounts for the interaction between the window and the wall. Cappelletti et al. [28] proposed to express heat losses associated with an installed window by an overall, two-dimensional U_{2D}-value.

Summarizing, in a building envelope in addition to single thermal bridges more complex multiple thermal bridges often occur. In the literature, guidelines on how to numerically predict heat losses due to single thermal bridging, multiple thermal bridging and thermal bridging associated with windows and their installation can be found. However, they apply to the building design stage where information about the structure is available. At this stage, no construction/installation errors are considered so the thermal bridges are designed for their perfect performance. However, once a building is constructed, the performance may vary from that predicted and ideally should be evaluated based on field measurements. Such measurements would reveal construction/installation errors and deterioration of materials over time. Also, commonly for older buildings, the building envelope structure is unknown making them unsuitable for numerical simulations.

As pointed out earlier, to achieve overall energy savings in the building sector, the industry should put particular emphasis on retrofitting the existing building stock. In-situ measurements of the existing building thermal performance before and after retrofitting are necessary to define the actual thermal improvement. Quantitative ITT has been shown to be an accurate and efficient approach for quantifying the heat loss through linear thermal bridges [21]. However, the methodology has been only validated on regular single thermal bridges with gentle temperature gradients. This study investigates the applicability of the ITT methodology to more realistic situations occurring in buildings. The response of thermal bridges located in close proximity to each other, often with steep gradients in the surface temperature distribution, is investigated. The testing includes complex scenarios, such as multiple linear thermal bridges and window installations. The latter is multifaceted heat loss system, comprising heat losses via glazing, frame, the connection between frame and glazing and heat losses around the window due to installation. In the methodology presented in this paper, the whole installed window is treated as a unit and the additional heat loss through the building component due to the window system is quantified. To do this a new window thermal transmittance or M-value is introduced.

Indoor thermography is used in this study, as it has been shown [16,17] that the indoor ITT is more suitable for thermal bridge detection than the outdoor ITT. The proposed methodology is applied to test specimens containing multiple thermal bridges, which were tested in controlled conditions in a hot box device [29]. Initially, specimens containing parallel thermal bridges are investigated to determine the interaction effects. More complex multiple bridging is then examined using specimens containing window elements to demonstrate the applicability of the approach to these situations. In addition, two different numerical approaches, heat transfer finite element (FE) and computational fluid dynamics (CFD) analysis that are validated against the hot box measurements, are used to model the thermal performance. The numerical predictions serve as additional checks on the validity of the ITT approach.

2. Experimental study

To investigate the suitability of the quantitative ITT approach for multiple thermal bridging heat loss assessment, testing of a number of specimens was carried out. First, the thermal performance of specimens, with multiple parallel thermal bridges at different spacings, was examined. This was followed by testing of specimens containing different window elements displaying more complex thermal bridging behavior. Tests were performed in a hot box under steady-state conditions. The hot box device is located in Cracow University of Technology, Faculty of Environmental Engineering, Poland.

2.1. Experimental procedure

The experiment was performed in the hot box, consisting of two climatic chambers, simulating indoor and outdoor conditions. Fig. 1 shows the experimental arrangement. First, the hot box testing was completed, as described in Section 2.3. Afterwards, the thermographic survey was performed, as described in Section 2.4. Both types of testing were accomplished under the same controlled, environmental conditions. Generally, the air temperature in the hot chamber was kept at about 25 °C and in the cold chamber at about −5 °C.
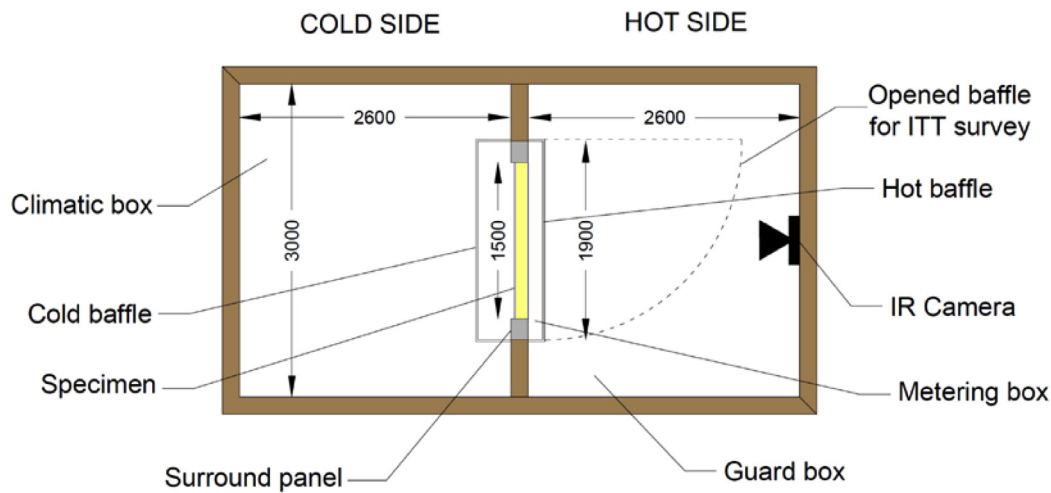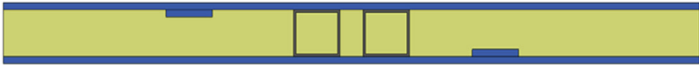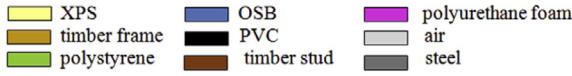
Fig. 1. Geometry of hot box.

Table 1
Geometries of test specimens.

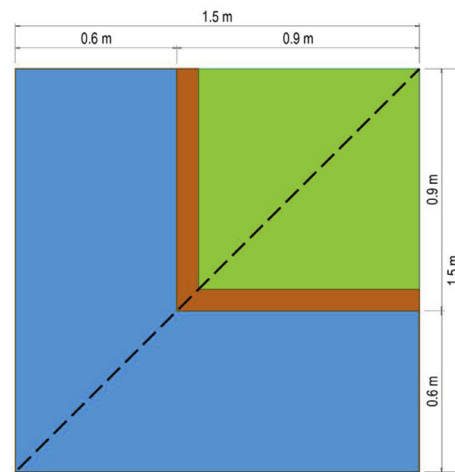## 2.2. Test specimen description

Four specimens, 1.5 m long and 1.5 m high, containing thermal bridges were tested. Geometries of the specimens are presented in Table 1. All specimens consist of structural insulated panels (SIPs) with total thicknesses of 130 mm. Each SIP panel consists of 100 mm thick low conductivity extruded polystyrene insulation (XPS) boards with 15 mm thick oriented strandboard (OSB) sheathing on both sides. Specimens 1 and 2 contain parallel thermal bridges created by steel square hollow (SHS) sections 100 mm ×

100 mm × 5 mm running from the top to bottom of the specimens. Specimen 1 contains two parallel thermal bridges positioned 50 mm apart which is less than the specimen thickness. Specimen 2 contains two steel square hollow sections (SHS) situated 300 mm apart from each other, which is greater than the thickness of the component. Specimens 3 and 4 contain window elements. Specimen 3 has a window with a timber frame whereas Specimen 4 has a window with a PVC frame. For experimental purposes, the window glazing has been replaced with polystyrene, in accordance with the standard EN ISO 12412-2 [30] for testing the thermal per-

Fig. 2. Specimen 3 mounted into the hot box surround panel (a) and Specimen dimensions (b).

formance of window frames. The 30 mm thick polystyrene sheet has a *U*-value of approximately 1 W/m^{2}K and is thermally-similar to double glazing. Fig. 2. shows Specimen 3 mounted into the hot box surround panel. Additionally, a plain Specimen 5, with the same structure but without any thermal bridge was tested to enable the evaluation of the thermal bridging heat loss for Specimens 1–4.

2.3. Hot box measurements

The hot box testing has been carried out in accordance with the EN ISO 8990 [29] standard. The hot side of the system simulates indoor environmental conditions and the cold side simulates outdoor environmental conditions. The construction of the hot box includes baffles to keep the air temperature and the air velocity uniform along the specimen surfaces. Specimens 1–5 were placed in sequence into a surround panel. To ensure that there was no air infiltration, silicone sealant and polystyrene foam insulation with low thermal conductivity (0.030 W/mK) were used to seal the

junction between the surround panel and the specimen. The joints were checked using the IR camera to ensure that sealing was correctly carried out. Then a metering box was fastened to the hot side of the surround panel and covered the whole area of the specimen (Fig 3). The aim of metering box is to ensure that the air temperature along the whole specimen is uniform. To obtain this, an air stream with very low velocity of 0.1 m/s is directed downward (inverted convection) between the hot baffle and the hot surface of the specimen throughout the test. The metering box is equipped with apparatus to measure the heat loss through the specimen. Fig. 1 shows the metering box situated in the guard box on the hot side. This arrangement minimizes the heat flow rate through the metering box walls.

On the cold side of the specimen, an isothermal cold baffle was attached where a wind velocity of approximately 1.50 m/s was induced. Two thermocouples were attached to the hot surface. On specimens with parallel thermal bridges (Specimen 1 and 2) they were placed in the mid-height of a specimen, one outside the thermal bridge zone of influence (S1) and one in the middle of one

Table 2
Hot box measurements.

Parameter	Unit	Specimen 1	Specimen 2	Specimen 3	Specimen 4	Specimen 5
T_e	°C	−4.85	−4.84	−4.88	−4.89	−4.91
T_i	°C	24.67	24.57	24.51	24.51	24.81
$T_{se,b}$	°C	−4.91	−4.91	−4.93	−4.89	−4.94
$T_{si,b}$	°C	24.02	23.98	23.94	23.91	24.53
T_{ni}	°C	24.23	24.16	24.12	24.09	24.62
T_{ne}	°C	−4.87	−4.86	−4.90	−4.89	−4.93
w_e	m/s	1.54	1.49	1.51	1.48	1.47
w_i	m/s	0.1	0.1	0.1	0.1	0.1
T_{S1}	°C	23.59	23.44	23.74	23.74	23.60
T_{S2}	°C	16.94	17.24	20.6	20.58	23.68
Φ	W	44.51	45.53	44.97	45.58	24.63

Fig. 3. Metering box fastened to the surround panel.

of the thermal bridges (S2). On specimens containing a window element (Specimen 3 and 4) the thermocouples were placed on the area not affected by thermal bridges, S1 on the SIP panel and S2 on the polystyrene. After a few hours, steady state conditions were achieved, and they were maintained throughout testing. At this stage, the hot box measurements were taken. Based on these measurements, the heat transferred through the specimen and surround panel was defined. A more detailed description of the hot box measurement procedure can be found in [21].

During the testing, data such as air temperatures, surface temperatures provided by thermocouples S1 and S2, air velocities, heat power input to the hot box were measured and recorded by the AMR Ahlborn Wincontrol system. These are summarized in Table 2.

In Table 2, environmental temperatures on the cold and on the hot sides (T_{ne} and T_{ni}, respectively) were obtained as a weighting of air temperatures recorded during testing (T_e and T_i) and baffle surface temperatures ($T_{se,b}$ and $T_{si,b}$). This was necessary as, according to EN ISO 8990 [29] and ISO 12567-1 [25], for calculations based on the heat flow rate measured in a hot box, an environmental temperature T_n should be used. The full procedure for obtaining the environmental temperature T_n is described in [21].

Before commencement of hot box testing, the device was calibrated in accordance with EN ISO 8990 [29] as described in [21]. The calibration process enables the quantification of how much heat has been transmitted via the surround panel, the specimen edges and via the specimen itself. The surface heat flux, $\dot{q}_{sp}$, and the heat flow rate through the whole specimen, $\dot{Q}_{sp}$, of each tested specimen was calculated using the equations below.

$$\dot{q}_{sp} = \frac{\Phi_{in} - \Phi_{sur,\,p} - \Phi_{edge}}{A} \tag{1}$$

$$\dot{Q}_{sp} = \dot{q}_{sp} A \tag{2}$$

After testing the plain specimen, the thermal bridge heat loss was obtained. The heat loss via parallel thermal bridges (Speci-

mens 1 and 2) is expressed by thermal bridging heat flow rate q_{TB} and was obtained using Eq. (3). This heat loss is the difference between the heat flow rate for specimens containing thermal bridges, $\dot{Q}_{sp}$, and the uniform heat flow rate for the plain Specimen 5, $\dot{Q}_{plain}$, divided by the specimen height H_{sp}. By dividing q_{TB} by the environmental temperature difference on each side of the specimen, the Ψ-value is obtained (Eq. (4)). For Specimens 3 and 4, the heat loss associated with the presence of the window is expressed by the thermal bridging heat flow rate $\dot{Q}_{TB}$ and was calculated using Eq. (5), as the difference between the heat flow rate for specimens containing thermal bridges, $\dot{Q}_{sp}$, and the uniform heat flow rate for Specimen 5, $\dot{Q}_{plain}$. A window thermal transmittance or M-value is introduced to describe the total additional heat lost from the building element due to the window element per unit temperature difference on each side of the element and is expressed in W/K. The M-value for the test specimens is found by dividing $\dot{Q}_{TB}$ by the environmental temperature difference between the hot and cold chambers (Eq. (6)).

$$q_{TB} = \frac{\left(\dot{Q}_{sp} - \dot{Q}_{plain}\right)}{H_{sp}} \tag{3}$$
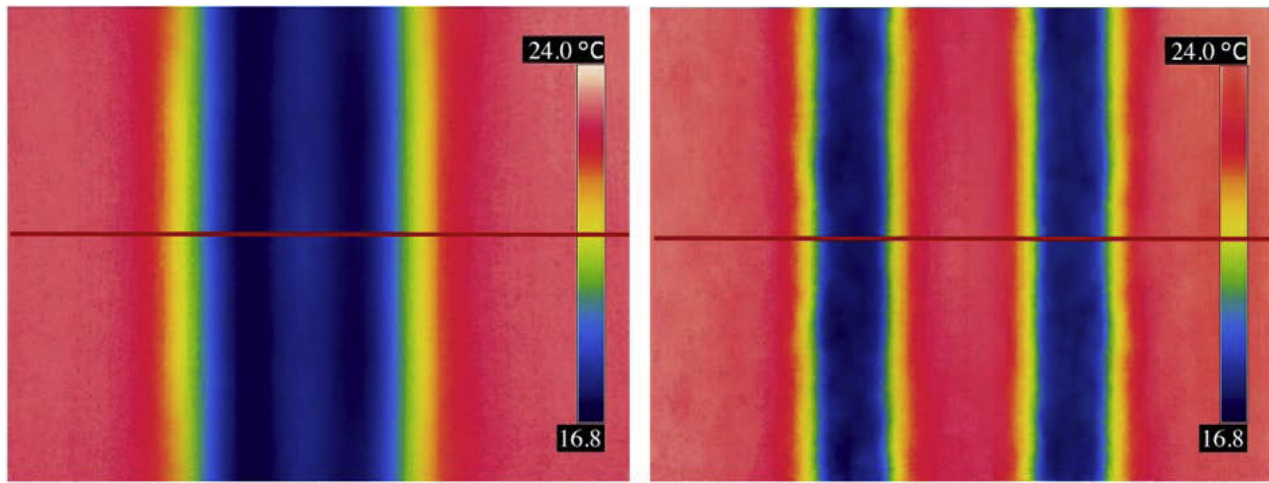
$$\Psi = \frac{q_{TB}}{(T_{ni} - T_{ne})} \tag{4}$$

$$\dot{Q}_{TB} = \dot{Q}_{sp} - \dot{Q}_{plain} \tag{5}$$
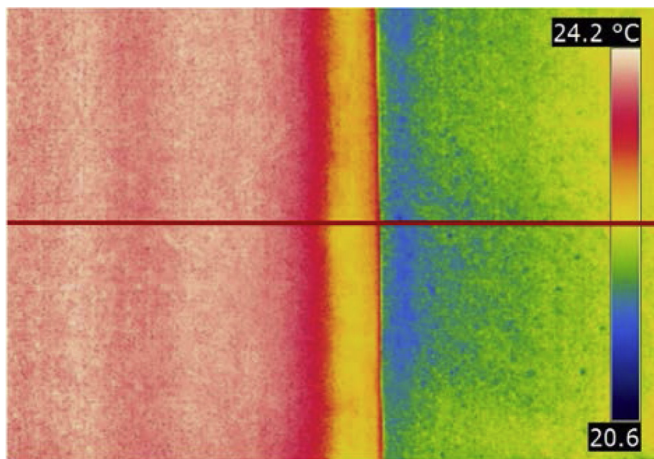
$$M = \frac{\dot{Q}_{TB}}{(T_{ni} - T_{ne})} \tag{6}$$

The uncertainty of the calculated results arising due to measurement errors is estimated using the error propagation rule [31–33]. The q_{TB}, Ψ-value, $\dot{Q}_{TB}$ and M-value uncertainties are linked to the measurement errors of air temperatures, surface temperatures, heat power input to the hot box, and specimen dimensions, which were 0.3 K, 0.3 K, 0.3 W and 0.001 m, respectively. The uncertainty (u) of q_{TB}, Ψ-value, $\dot{Q}_{TB}$ and M-value obtained from hot box tests are given in the Results and discussion section.

2.4. Thermographic survey

The ITT measurements were taken on the hot surfaces immediately after the hot box experiment and after removing the baffle from the hot side of the specimen. The infrared images (IR images) were taken with a Flir T335 IR camera with a 25° lens, 320 × 240 resolution and a spectral range 7.5–13 μm. The survey environmental conditions were the same as for the hot box testing given in Table 2. Fig. 4 presents examples of thermograms for Specimens 1 and 2. This figure demonstrates that the two thermal bridges in Specimen 1 interact so strongly with each other that they practically act as a single thermal bridge. Fig. 5 shows a sample IR image

Fig. 4. Sample IR images for Specimen 1 (left) and of Specimen 2 (right). (For interpretation of the references to color in this figure, the reader is referred to the web version of this article.)

Fig. 5. IR image of Specimen 3 with a timber frame window.

taken on Specimen 3 containing a timber frame window. The surface temperatures are disturbed by the window components and junctions including the window frame, the polystyrene glazing replacement, and the connections between the window frame and the wall and between the frame and polystyrene. A sequence of IR images of each tested specimen has been taken. Using each image, an IR line was created using the temperature data from three adjacent horizontal rows of pixels. Each temperature on the IR line represents the average of the temperatures of the middle pixel and the eight surrounding pixels. This temperature averaging resulted in smooth transition of temperature values from one pixel to another. From all IR lines for each specimen, a mean IR line was formed. For parallel multiple thermal bridges (Specimens 1 and 2), IR lines were created using rows of pixels at mid-height of the IR image. The mean IR line shows satisfactorily the full temperature distribution across the specimen and, since the specimens were symmetrical, it was created only for one-half of the specimen. The location of the IR lines is shown in red in Fig. 4. Considering specimens with window elements (Specimens 3 and 4), the IR line was created using rows of pixels at the mid-height of the vertical window frame, as indicated in Fig. 6. The methodology described in the next section is applied to the mean IR line.

3. Application of ITT methodology to quantifying the heat loss through multiple thermal bridges and through window elements

In the current study, the methodology, originally developed for single thermal bridge assessment [21], is applied to evaluate the heat flow rate through multiple linear thermal bridges and through complex thermal bridges such as window elements. The methodology is based on the surface energy balance applied to the internal face of the building envelope component containing the thermal bridge. Using this balance rule, the heat flow rate for each pixel (q_x) on the IR line can be obtained using the equation below.

$$q_x = l_x[(h_{cx} + h_{rx})(T_i - T_{sx})] \tag{7}$$

Surface temperatures on the IR line, located at a significant distance from the thermal bridge are not impacted by the thermal bridge. The temperature of any pixel in this region is used to calculate the uniform heat flow rate q_{xu}, using also Eq. (7). This is used to predict the heat flow rate of the same building component but without a thermal bridge.

The thermal bridge heat flow rate for each pixel q_{xTB} is then found using the equation below.

$$q_{xTB} = q_x - q_{xu} \tag{8}$$

The thermal performance of multiple thermal bridges is described by the thermal bridge heat flow rate q_{TB} and the Ψ-value. These values describe heat loss in Watts per unit height. The q_{TB} is obtained by summing the q_{xTB} for all pixels on the IR line.

$$q_{TB} = \sum q_{xTB} \tag{9}$$

Finally, the Ψ-value is obtained by dividing this thermal bridge heat flow rate q_{TB} by the difference in indoor and outdoor air temperatures.

$$\Psi = \frac{q_{TB}}{(T_i - T_e)} \tag{10}$$

In the current methodology, the heat loss due to the installed window is expressed as an additional heat loss through the building envelope and described by the thermal bridging heat flow rate $\dot{Q}_{TB}$. $\dot{Q}_{TB}$ describes the complex additional heat loss through the zone affected by the presence of the window and is expressed in Watts. This complex heat loss accounts also for heat losses around the window due to installation that can, especially in older buildings, significantly impact the window thermal performance. The other reason for including the installation Ψ-value in $\dot{Q}_{TB}$ is
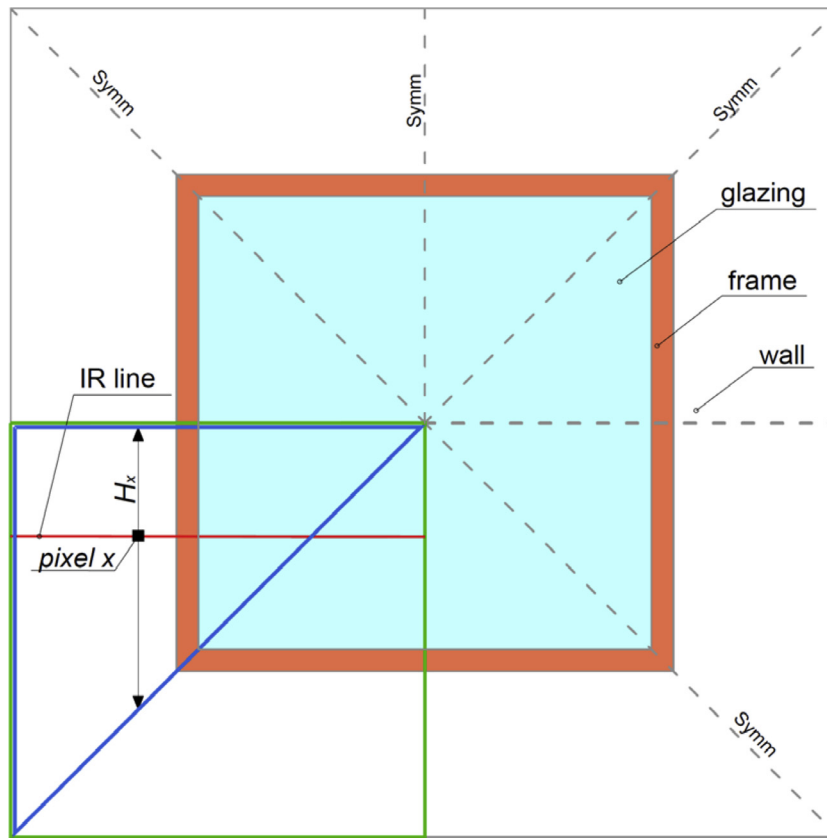
Fig. 6. Geometry of a window installed into a wall. Tested section outlined in green, section for calculation outlined in blue. (For interpretation of the references to color in this figure legend, the reader is referred to the web version of this article.)

the infeasibility of separating the thermal bridges located close to each other while performing the ITT assessment.

Due to the window geometry, the surface temperatures at the corners of the window frame are slightly different to those along the rest of the frame. To investigate how this influences the $\dot{Q}_{TB}$, numerical analyses were carried out. They included windows with: (i) polystyrene 'glazing' and glass double glazing, (ii) two types of frames, timber and PVC and (iii) three different types of spacers, namely, steel, aluminium and polypropylene. The window thermal bridging heat flow rate $\dot{Q}_{TB}$ was then calculated using two approaches. First, it was derived from the entire window/wall surface. In the second approach, an assumption was made that the surface temperatures are the same along the perimeter of the window frame and $\dot{Q}_{TB}$ was determined from a line of temperatures across the frame. For the models of windows with polystyrene 'glazing', the maximum deviation of $\dot{Q}_{TB}$ calculated using this assumption from that derived using the entire surface accounted to + 1.8%. This simplification had a smaller impact on the $\dot{Q}_{TB}$ of the double-glazed windows, where the maximum deviation between $\dot{Q}_{TB}$ calculated using this assumption from that derived from the entire surface was + 1.0%. In the all analyzed cases, the surface temperatures were higher in the corner of the frames due to change of the geometry. Therefore, using the assumption that they are the same along the whole frame perimeter results in a slight overestimation of $\dot{Q}_{TB}$. To make the methodology practical and quick, it was decided to introduce the approximation that the surface temperatures are the same along the frame perimeter. With this simplification, the heat loss via the window frame and glazing together with connections between the frame and wall and between the frame and glazing may be determined from a single IR line.

In a similar manner, the heat flow rate for each pixel q_x and the thermal bridge heat flow rate for each pixel q_{xTB} on an IR line containing the wall unit and all window components are calculated using Eqs. (7) and (8), respectively. For the tested window specimens, due to diagonal symmetry, it is only necessary to carry out the analysis on half of the specimen as outlined in blue in Fig. 6. The IR line for half of the specimen is shown in red on Fig. 6. To determine the $\dot{Q}_{TB}$ associated with the installed window, each q_{xTB} is multiplied by an associated height H_x (Eq. (11)). Fig. 6 shows H_x corresponding pixel x. By summing the $\dot{Q}_{xTB}$ over all pixels on the IR line (Eq. (12)) and multiplying by 2, the thermal bridging heat loss via the window element for the full specimen is calculated. By dividing the $\dot{Q}_{xTB}$ by the air temperature difference on each side of the specimen, window thermal transmittance M-value is obtained, using Eq. (13).

$$\dot{Q}_{xTB} = q_{xTB} * H_x \tag{11}$$

$$\dot{Q}_{TB} = \sum \dot{Q}_{xTB} * 2 \tag{12}$$

$$M = \frac{\dot{Q}_{TB}}{(T_i - T_e)} \tag{13}$$

The determination of heat flow rate for each pixel using Eq. (7) requires accurate calculation of the heat transfer coefficients. It was shown by O'Grady et al. [21] that this approach contributed to improved accuracy when compared with results obtained with a uniform convective coefficient. Therefore, in the current methodology, precise calculation of the convective heat transfer coefficients h_c for each pixel x is carried out using the Nusselt

Table 3
Material properties applied to numerical simulations.

Property	Unit	Symbol	Material				
			OSB/timber	Steel	XPS	Polystyrene	Polyurethane foam
Conductivity	W/(mK)	k	0.13 [37]	50.2 [38]	0.033 [39]	0.037 [21]	0.030 [40]
Density	kg/m^3	ρ	600 [37]	7850 [41]	33 [39]	24 [42]	30 [43]
Emissivity	–	ε	0.93	–	–	–	

number Nu.

$$h_{cx} = \frac{Nu_x \, k_x}{l_{ch}} \tag{14}$$

where l_{ch} is the characteristic length over which h_c applies and k is the thermal conductivity of the air. Nu is the Nusselt number which is a dimensionless surface temperature gradient [34]. In the indoor environment, it can be evaluated using the Churchill–Chu correlation (Eq. (15)) that was originally developed for a vertical plate.

$$Nu_x = \left\{ 0.825 + \frac{0.387 Ra_x^{\;1/6}}{\left[1 + \left(\frac{0.492}{Pr_x} \right)^{9/16} \right]^{8/27}} \right\}^2 \tag{15}$$

The Prandtl number (Pr) is the ratio of kinematic viscosity to thermal diffusivity of the air. The Rayleigh number (Ra) characterizes free convection flow by describing the relationship between buoyancy and viscosity of air and is obtained for each pixel using the equation below:

$$Ra_x = \frac{g\beta_x(T_i - T_{sx})l_{ch}^3}{\nu_x \, \alpha_x} \tag{16}$$

The radiative heat transfer coefficient h_r is also evaluated for each pixel on the IR line using the equation below

$$h_{rx} = \varepsilon\sigma \left(T_{sx} + T_i \right)\left(T_{sx}^2 + T_i^2 \right) \tag{17}$$

The surface emissivity ε used in Eq. (17) was measured in-situ with the ITT, using the contact method, in accordance to ISO 18434-1 [35]. This emissivity was used for both the experimental calculation and the numerical simulations and is given in Table 3.

Eqs. (7) and (17) are used under the assumption that the building indoor air temperature T_i is constant and very similar to the surrounding temperature T_{sur} which is very often the case. The equations that are appropriate for other cases can be found in [21].

4. Numerical studies

Numerical studies of the tested specimens were undertaken to allow for comparison of the ITT surface temperature distributions with the simulated ones. As only two thermocouples were used during the hot box testing, a comparison with the experimental temperatures was limited to two spot temperatures. In addition, since the numerical approach is commonly used in practice to assess thermal bridging where the wall construction details are known, it is useful to compare this approach with the ITT results.

The thermal bridge heat flow rate q_{TB}, Ψ-value of the linear thermal bridges and $\dot{Q}_{TB}$ and M-value of window elements are also determined. For specimens with linear thermal bridges two types of simulations are investigated: finite element (FE) steady-state heat transfer analysis using the ABAQUS package [36] and computational fluid dynamic (CFD) analyses using Ansys Fluent. The results derived from these two types of simulations suggest that FE steady-state heat transfer analysis is sufficiently accurate for thermal bridging heat loss evaluation. Therefore, for window thermal bridging evaluation, only this type of simulation is carried out.

4.1. Two-dimensional heat transfer finite element models in Abaqus Standard

Two-dimensional (2D) steady-state FE heat transfer numerical simulations were carried out for Specimens 1 and 2 containing linear parallel thermal bridges and for plain Specimen 5, under the tested environmental conditions. The analyses were carried out with air temperatures and wind velocities mirroring the conditions of the hot box experiment presented in Table 2. Simulations included the whole 1.50 m specimen length. Material properties used for the models are presented in Table 3.

The type of element used was a 4-node linear heat transfer quadrilateral (DC2D). A mesh convergence study resulted in an element size of 0.005 m being selected. With this element size, the total heat flow rate q_{tot} varied by only 0.25% from that with a coarser mesh. A finer element size of 0.001 m was used for the steel post, as the post was only 0.005 m thick. Fig. 7 shows part of the meshed Specimen 1 in the vicinity of the steel posts.

Variable indoor convective boundary conditions were implemented in the simulations. These coefficients were evaluated using Eq. (14), initially from nodal temperatures on the hot surface obtained in a simulation with constant h_{ci}. Based on the predicted temperatures the convective coefficients were updated, and the analysis was repeated. After a further iteration convergence was achieved. Fig. 8 shows the calculated surface convective coefficients for each specimen. As can be seen in this figure, h_{ci} is constant in the plain part of the specimens, outside the thermal bridge zone of influence, but increases significantly by about 1.3 W/m^{2}K for all specimens at the thermal bridge location. Local disturbance in the h_{ci} values, between 1.05–1.15 m for Specimen 1, correspond to the location of OSB connectors used to join two sheets of external OSB in the SIP manufacturing process. The external convective coefficient h_{ce} was calculated for the wind velocities presented in Table 2, using Eq. (18), given by standard EN ISO 6946 [44].

$$h_{ce} = 4 + 4w \tag{18}$$

The FE software used in this study calculates surface radiation using the Stefan–Boltzmann law using the input value of surface emissivity given in Table 3, which was derived from measurements as described above.

The total heat flow rate for the specimen per unit height, q_{tot}, is obtained directly as an output from the simulation. To obtain the thermal bridge heat flow rate q_{TB}, the uniform heat flow rate q_u of plain Specimen 5 was simulated. The q_{TB} was obtained from the equation below.

$$q_{TB} = q_{tot} - q_u \tag{19}$$

The Ψ-value was then calculated in accordance with Eq. (10).

4.2. Three-dimensional numerical simulations in Ansys Fluent

The Ansys Fluent numerical tool was used for the CFD calculations. Using this program, the behavior of systems, processes and equipment involving the flow of gases and liquids, heat and mass transfer can be simulated. It can also be used for simulating energy efficient building systems and components including building
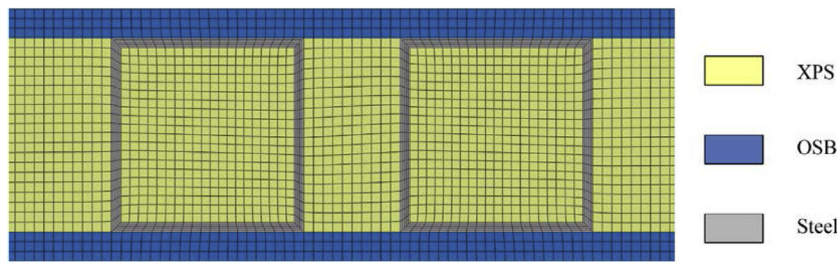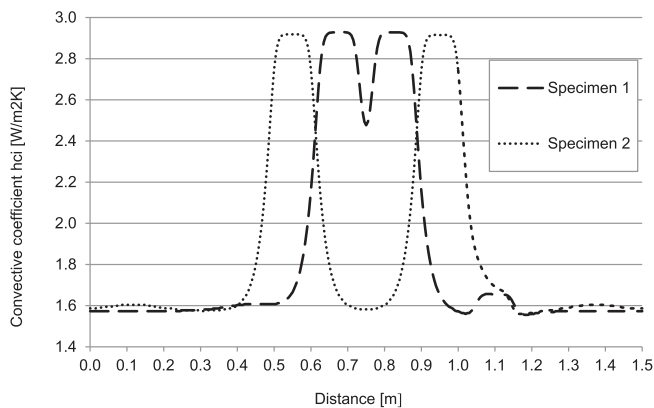
Fig. 7. A part of meshed Specimen 1.

Fig. 8. Indoor convective coefficients.

Table 4
Air thermal properties applied for the calculations.

T [°C]	ρ [kg/m³]	λ [W/(mK)]	c_p [J/(kgK)]	μ [kg/(ms)]
−10	1.342	0.0236	1005.0	$1.67 \cdot 10^{-5}$
0	1.293	0.0244	1005.0	$1.72 \cdot 10^{-5}$
10	1.247	0.0251	1005.0	$1.76 \cdot 10^{-5}$
20	1.205	0.0259	1005.0	$1.81 \cdot 10^{-5}$
30	1.165	0.0267	1005.0	$1.86 \cdot 10^{-5}$

Table 5
Boundary conditions.

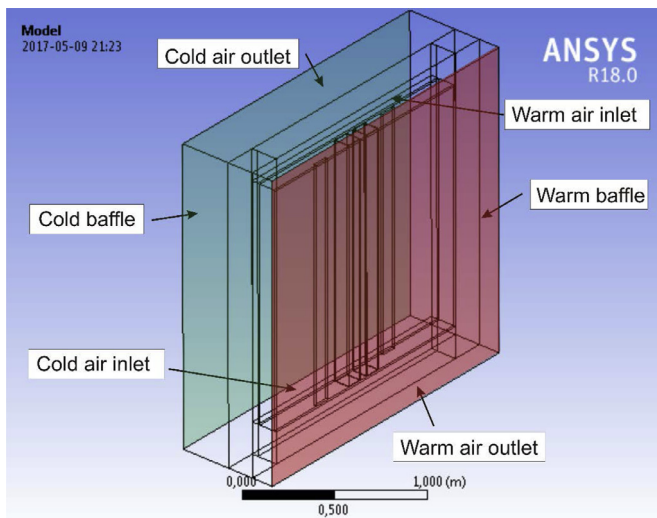| Specimen	$T_{se,b}$ [°C]	$\dot{m}_e$ [kg/s]	$T_{inlet,e}$ [°C]	$\dot{m}_e$ [kg/s]	$T_{inlet,i}$ [°C]
1	−4.91	1.337	−7.05	0.0346	26.05
2	−4.91	1.298	−7.35	0.0346	26.15
5	−4.95	1.239	−5.15	0.0346	24.78

Fig. 9. The 3D view of Specimen 1 with surrounding elements. (For interpretation of the references to color in this figure, the reader is referred to the web version of this article.)

inlet and outlet and baffles is given in Fig. 9. The cold baffle is shown in green and warm baffle in red.

The same material properties, listed in Table 3, were applied as for 2D FE simulations. Additionally, the thermal conductivity of the surround panel made of Styrofoam was assumed to be 0.033 W/(mK) and its surface emissivity 0.92. For the hot and cold baffles, a surface emissivity is 0.95 was used. Air thermal properties were assumed to be piecewise linear between the values presented in Table 4.

A mass flow inlet of warm air at a uniform temperature at the top of the model and warm air outlet at the bottom of the model simulates the inverted convection in the hot box during the testing. The cold baffle surface was assumed to be isothermal with the mean surface temperature known from measurements. The warm baffle surface was defined as adiabatic because the baffle was the hot box wall; hence no heat was transferred through the hot box walls during the measurements. Boundary conditions for all three specimens are given in Table 5. The warm air inlet and the cold air inlet temperatures $T_{inlet,i}$ and $T_{inlet,e}$, respectively, were measured during the experiment using three thermocouples for each case. The inlet temperatures were the average values from these three thermocouples.

partition's thermal performance [45]. The program implements the finite volume method.

In this section, geometrical 3D models of tested Specimens 1 and 2 with linear thermal bridges and of a plain Specimen 5 are introduced. The specimens' geometries are shown in Table 1. The 3D simulations mirror the hot box tests and take into account not only the specimens themselves but also the supporting panel (into which the specimens are mounted), the air flowing along the specimens on both sides and the baffles around both sides of the specimens forming the air channel. A 3D view of the model for Specimen 1 mounted into the surrounding Styrofoam panel with an air
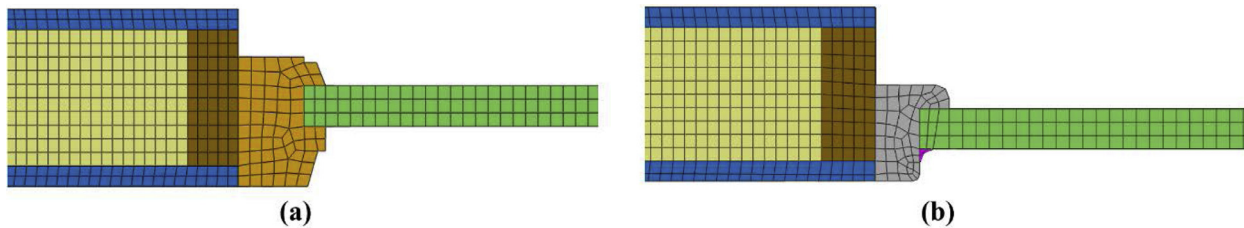
4.2.1. Mesh and model settings

All calculations were performed with a mesh of about 4.5 million elements. The mesh qualities were checked for: aspect ratio (max. 1:27) and skewness (max. 0.94). Their values should not exceed the limiting values of 1:35 and 0.95, respectively [45].

The settings for the finite volume CFD model for the convective and radiative heat transfer are listed in Table 6.

The heat flow rate through specimens containing thermal bridges 1 – 2 ($\dot{Q}_{sp}$) and heat flow rate through the plain Specimen 5 ($\dot{Q}_{plain}$) was derived from the models. Then, using Eqs. (3) and (10), q_{TB} and Ψ-value were calculated, respectively.

Table 6
CFD model settings.

Solver	Stationary	
Viscous model	$k–\varepsilon$	
Air thermal properties	Density, conductivity and dynamic viscosity	Piecewise-linear
	Specific heat	Constant
Discretization schemes	Gradient	Least squares cell based
	Pressure	Standard
	Momentum	Second order upwind
	Turbulent kinetic energy	Second order upwind
	Turbulent dissipation rate	Second order upwind
	Energy	Second order upwind
Radiation model	Discrete Transfer Radiation Model	

Fig. 10. Part of mesh of model for Specimen 3 (a) and Specimen 4 (b). (For colour legend, refer to Table 1).

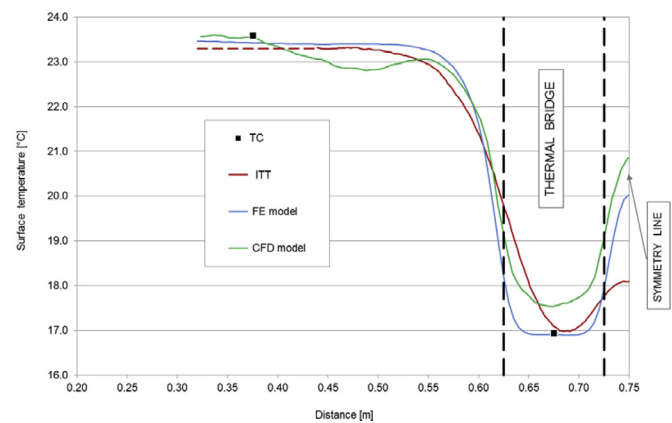### 4.3. Three-dimensional heat transfer finite element models in Abaqus Standard

Results of the modeling of Specimens 1 and 2, presented in Section 5, show that it is sufficient to perform steady-state heat transfer FE simulation for multiple thermal bridging assessment. Therefore, for Specimens 3 and 4 containing window thermal bridging only this type of simulation was undertaken. Because of the complexity of the window geometry, a 3D model was created. The analyses were carried out with the same air temperatures and wind velocities as the hot box experiment (Table 2). Material and air properties used for the models are presented in Tables 3 and 4, respectively. For Specimen 4, the thermal properties of the PVC frame were calculated as the area-averaged values for PVC and air. As the window specimen had diagonal symmetry, only one half of the specimen was modelled.

The type of element used was a 20-node quadratic heat transfer brick (DC3D20), with an element size 0.01 m. With this size, mesh convergence was found, as the heat flow rate of the whole specimen $\dot{Q}_{sp}$ differed by only 0.15% from that with a coarser mesh. Fig. 10 shows the FE meshes for Specimen 3 (a) and Specimen 4 (b).

From the 3D FE simulations, the thermal bridging heat flow rate $\dot{Q}_{TB}$ was calculated using Eq. (5), as the difference between the heat flow rate for specimens containing thermal bridges, $\dot{Q}_{sp}$, and the uniform heat flow rate for Specimen 5, $\dot{Q}_{plain}$. Then the thermal transmittance associated with window system M-value was calculated using Eq. (13).

5. Results and discussion

In this section, the results from the thermographic survey and from 3D CFD, 2D FE and 3D FE simulations are presented and compared with the hot box measurements. All experimental results are given together with their uncertainties *(u)*. The uncertainty of the ITT results is expressed in terms of the experimental standard deviation *(SD)*. The *SD* is calculated from series of five ITT measurements to characterize the dispersion from the mean value, according to Guide 98-3 [46]. As only one set of measurements for each specimen was taken using the hot box and thermocouples, the uncertainties are calculated, as described in Section 2.3, for the hot

Fig. 11. Surface temperature on the warm side of Specimen 1 obtained from thermocouples, the ITT, 2D FE and 3D CFD models.

box and taken as the measurement accuracy provided by the manufacturer for the thermocouples.
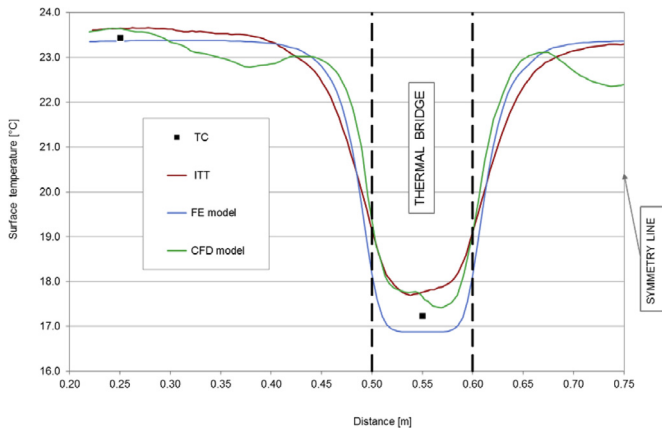
5.1. Linear parallel thermal bridges

Results obtained from measurements and from numerical simulations of Specimens 1 and 2 containing parallel linear thermal bridges are presented and discussed. The results include surface temperatures, thermal bridge heat flow rate q_{TB} and linear thermal transmittance Ψ-value.

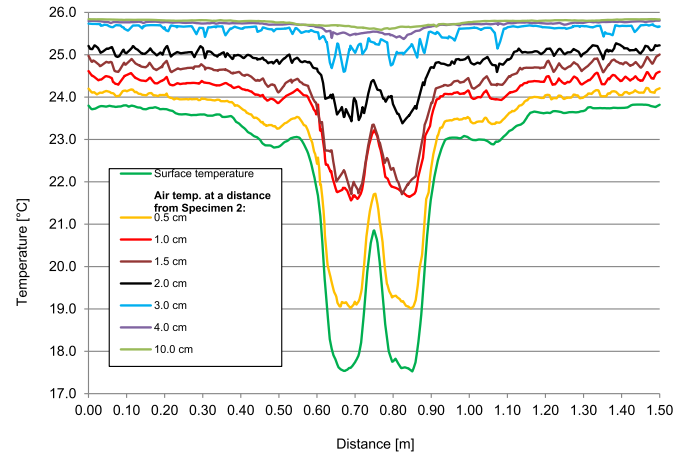#### 5.1.1. Surface temperature distributions

Figs. 11 and 12 show the temperature distributions along a horizontal line at the specimens' mid-height on the hot surface. On these lines, two spot temperatures measured by thermocouples (TC) S1 and S2 during the hot box testing are marked. The temperature T_{S1} denotes the uniform surface temperature outside the thermal bridge zone of influence and temperature T_{S2} the surface temperature measured in the middle of thermal bridge. Table 7 presents these temperatures obtained from four different methods. Temperatures obtained by means of the ITT and from numerical simulations are compared to the temperatures measured by

Table 7
Surface temperatures comparison.

		Surface temperatures [°C]						Differences from TC [°C]		
		TC	u TC	ITT	SD ITT	FE model	CFD model	ITT	FE model	CFD model
T_{S1}	Specimen 1	23.59	0.30	23.30	0.21	23.43	23.55	−0.29	−0.16	−0.04
	Specimen 2	23.44	0.30	23.64	0.11	23.37	23.64	0.20	−0.07	0.20
T_{S2}	Specimen 1	16.94	0.30	16.98	0.06	16.91	17.54	0.04	−0.03	0.60
	Specimen 2	17.24	0.30	17.77	0.16	16.9	17.67	0.53	−0.34	0.43

Fig. 12. Surface temperature on the warm side of Specimen 2 obtained from thermocouples, the ITT, 2D FE and 3D CFD models.

Fig. 13. Surface and air temperatures distribution along the Specimen 2 at mid-height.

thermocouples. As can be seen in Figs. 11 and 12 and in Table 7, the uniform surface temperatures T_{S1} measured by the ITT and the thermocouples and obtained from numerical simulations are in excellent agreement. The maximum difference for T_{S1} between the thermocouple and ITT measurements was −0.29 °C for Specimen 1. The maximum difference between minimum surface temperatures in the middle of the thermal bridge T_{S2} was +0.60 °C and relates to the temperature obtained in CFD model for Specimen 1. These maximum differences between these values indicate a good agreement between all methods.

While considering the surface temperature at the symmetry line between the two thermal bridges in Specimen 1, an increase of around 3 °C from the temperature on the thermal bridge, T_{S2}, can be seen in all simulated temperatures. At the same point, the temperature recorded by the ITT increased by only 1 °C. While comparing the temperatures at the specimen symmetry line of Specimen 2, it can be seen that the temperatures obtained from FE simulations came back to the uniform temperature. This thermal behavior is in agreement with [23], which stated that thermal bridges situated further apart than the component thickness, do not influence each other. The temperature obtained by the ITT at the same point shows a value 0.34 °C lower than the uniform temperature T_{S1}. The fact that the uniform temperature has not been reached between the two thermal bridges indicates that the ITT recording shows a greater level of interaction between the thermal bridges. The thermal bridge zone of influence recorded by the ITT is in all cases greater than that simulated numerically, as it can be seen in Figs. 11 and 12. This difference was previously identified by Heinrich and Dahlem [15].

The differences in surface temperature distribution provided from numerical simulations can be explained in part by the different approaches used to account for convective boundary conditions along the hot specimen surface. In the 2D FE simulations, the indoor convective boundary conditions were applied using variable indoor convective coefficients correlated with surface temperatures. On the other hand, the 3D CFD simulations included the

baffles surrounding the specimen in the model and the boundary conditions were applied by specifying the air inlet and outlet properties, hence they account for convective movements along the specimen surfaces. This was done to reflect the test conditions in the hot box as closely as possible. The CFD simulations revealed that, due to the thermal bridge presence, the conditions between the specimen and the hot baffle did not stay uniform as shown in Fig. 13 for Specimen 2. The dark green line represents the surface temperatures whereas the other lines represent air temperatures at different distances from the specimen. This figure demonstrates the non-uniformity of the air while testing a specimen containing thermal bridges in the hot box and explains the presence of irregularities in the temperature profiles seen in Figs. 11 and 12. It should be pointed out that the ITT was performed after the hot box testing was completed and after the hot baffle was removed so the downstream flow along the specimen was no longer present. This may explain the difference between temperature distributions measured by the ITT and simulated in CFD models. Other factors influencing the accuracy of the numerically-predicted temperature distributions are errors in the assumed material properties and homogeneity, which may not fully reflect the actual conditions.

As can be seen in Figs. 11 and 12, the simulated thermal bridge zones of influence are smaller than those recorded by the ITT. As mentioned previously, this was also reported in a study by Heinrich and Dahlem [15] who attributed the difference to the boundary conditions assumed in the simulations. Using ITT or other in-situ measurements of temperatures such as thermocouples does not have this drawback. However, to obtain a complex surface temperature distribution of a component affected by thermal bridging, a significant number of thermocouples would be needed. For this purpose, the ITT is a much more suitable tool as it allows the full surface temperature distribution impacted by thermal bridging to be measured.

Table 8
Thermal bridge heat flow rate q_{TB} and linear thermal transmittance Ψ-value.

		q_{TB} and Ψ results						Deviation from hot box [%]		
		Hot box	U hot box	ITT	SD ITT	FE model	CFD model	ITT	FE model	CFD model
q_{TB} [W/m]	Specimen 1	7.41	0.28	7.04	1.61	7.54	8.33	−4.99	1.75	12.42
	Specimen 2	13.09	0.28	13.42	2.63	14.41	13.61	2.52	10.08	3.97
Ψ [W/mK]	Specimen 1	0.450	0.010	0.455	0.017	0.488	0.418	1.11	8.44	−7.11
	Specimen 2	0.474	0.010	0.507	0.090	0.496	0.412	6.96	4.64	−13.08

5.1.2. Thermal bridge heat flow rate q_{TB} and linear thermal transmittance Ψ-value

The thermal bridge heat flow rate q_{TB} and the linear thermal transmittance Ψ obtained from the hot box measurements and from the ITT, as well as those obtained from numerical simulations are presented in Table 8. The results from the ITT and from simulations are compared to the results from hot box, as reference values. The ITT results are calculated using variable convective coefficients, as described in Section 3.

Comparison of the results (Table 8) obtained according to proposed methodology using the ITT with those measured by the hot box shows good agreement. The percentage deviations between −5.0% and +2.5% for q_{TB} and between +1.0% and +7.0% for Ψ-values have been recorded. Considering the thermal bridge heat flow rate q_{TB} derived from numerical simulations for Specimen 1, the greatest deviation was +12.5% for CFD model. For Specimen 2, the q_{TB} derived from FE model had the highest deviation at +10.0%. When comparing the Ψ-values for Specimen 1, the greatest deviation was +8.5% for the FE model. The maximum deviation was −13.0% in the Ψ-value obtained from the CFD model for Specimen 2. In general, the maximum deviation of results derived from numerical simulations from the hot box measurements is greater than for the ITT results. This may be due to the boundary conditions input and the assumed thermal properties input to the simulations being different from the actual values. Also, in the numerical analysis, possible workmanship mistakes or inhomogeneities in the construction are not taken into account. On the other hand, the ITT method represents the results based on measurements thus represents the actual thermal performance of the specimen.

To define how the accuracy of ITT results is impacted by the pixel-based approach to determining the h_{ci} value, the Ψ-value of the tested specimens was also calculated using a constant value of h_{ci} equal to 2.5 W/m²K, in accordance with EN ISO 6946 [40]. Using the constant h_{ci} approach, the calculated Ψ-values deviate by 2.5% and 8.5% more that the values obtained using the variable approach for Specimens 1 and 2, respectively. This comparison confirms the correctness of approach presented in [21], where it was demonstrated that evaluation of surface coefficients for each pixel on the IR line improves the results accuracy.

5.1.3. Influence of the distance between parallel thermal bridges on Ψ-values

In this section, the influence of thermal bridges' positioning on the Ψ-value is presented and discussed. To observe the increase of heat loss caused by two thermal bridges located at different distances from each other, test results from a specimen containing a single thermal bridge (Specimen S), included in a study published in [21], are used as reference values. The first row of Table 9 presents Ψ-values for this specimen, multiplied by two to represent the influence of two independent non-interacting thermal bridges. The remaining rows give the differences between this Ψ-value and the Ψ-values evaluated for Specimens 1 and 2. The differences between Ψ-values are very small; however, some trends can be noticed. The Ψ-values for Specimen 1, situated 0.05 m apart, are lower than the Ψ-value of two single thermal bridges. In gen-

Table 9
Ψ-values in [W/mK] for thermal bridges at different spacing.

	Hot box	ITT	FE model	CFD model
Specimen S × 2	0.506	0.476	0.514	0.510
Specimen S × 2 – Specimen 1	0.056	0.021	0.022	0.092
Specimen S × 2 – Specimen 2	0.032	−0.031	0.014	0.098

eral, the heat loss increases when the distance between thermal bridges increases. However, the simulated values showing negligible differences between results predicted for thermal bridges located 0.05 m and 0.30 m apart. The Ψ-value measured by the ITT shows the greatest increase (11.5%) while extending the distance between the thermal bridges. The Ψ-value provided by the hot box measurement for Specimen 2 is 5% greater than the Ψ-value of Specimen 1. As demonstrated previously in Section 5.1.1, the ITT recorded stronger interaction between the thermal bridges at 0.05 m spacing than the simulation methods. Also, as can be seen in the temperature distribution of Specimen 2 in Fig. 12, the ITT still shows some degree of interaction between the thermal bridges at 0.30 m spacing whereas simulation methods do not reflect any interaction. This explains the greater increase of Ψ-values measured by the ITT than from the simulations.

When undertaking an assessment of thermal bridging using the ITT, adjacent bridges can be assumed to interact if the temperature between the bridges remains lower than the uniform surface temperature. In this case, the assessment of the two bridges should be included in the same analysis.

5.2. Window system thermal bridges

Experimental and numerical results for Specimens 3 and 4 containing window elements are presented and discussed. The temperatures, heat flow rates and window thermal transmittance results obtained from ITT measurement and from numerical simulations are compared with those obtained in the hot box device.

5.2.1. Surface temperature distributions on specimens with windows

Figs. 14 and 15 show the temperature distributions along horizontal lines across Specimen 3 and 4 at the mid-height of the vertical window frame on the hot surface. During testing, two uniform surface temperatures were measured by thermocouples (TC). The temperature T_{S1} recorded the uniform temperature on the wall surface (at a distance of 0.3 m from the left edge of the specimen) and T_{S2} on the polystyrene 'glazing' (at a distance of 0.9 m from the left edge of the specimen). The ITT temperature profile is the mean temperature determined from five individual thermograms (Lines IR 1–IR 5). In addition, the temperature distribution derived from the numerical simulations (FE model) is presented. These lines show how the presence of an installed window disturbs the uniform wall surface temperatures. As can be seen in these figures and in Tables 10 and 11, the surface temperature distribution measured by the ITT and the thermocouples and obtained from numerical simulations are in good agreement.
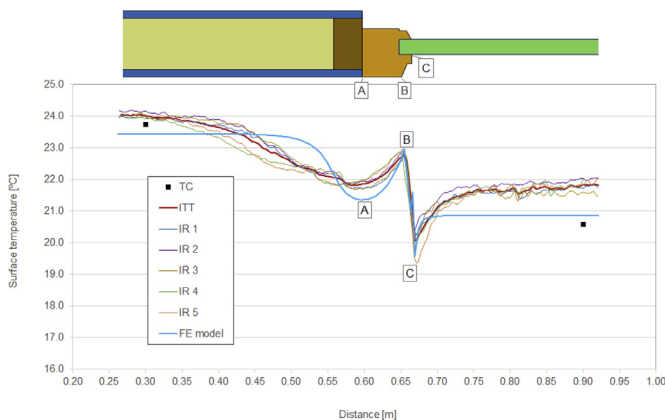
Considering the temperatures of points S1 and S2, it can be seen that the steady state temperature on the wall component

Table 10
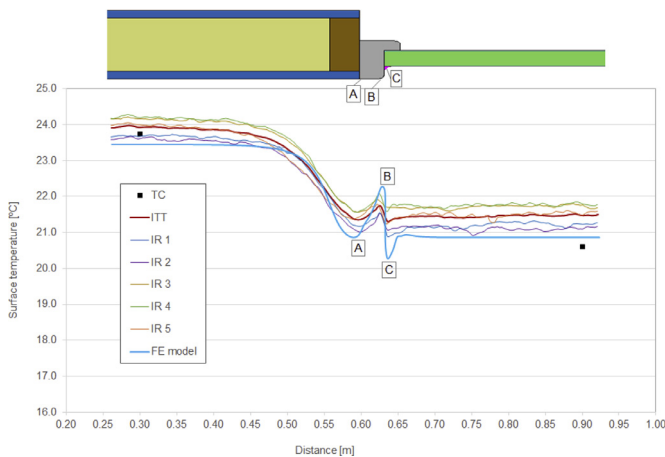Uniform surface temperatures T_{S1} and T_{S2} comparison.

		T_{S1} and T_{S2} [°C]					Differences from TC [°C]	
		TC	u TC	ITT	SD ITT	FE	ITT	FE
T_{S1}	Specimen 3	23.74	0.30	24.04	0.07	23.45	0.30	−0.29
	Specimen 4	23.74	0.30	23.95	0.24	23.45	0.21	−0.29
T_{S2}	Specimen 3	20.60	0.30	21.81	0.18	20.86	1.21	0.26
	Specimen 4	20.58	0.30	21.59	0.28	20.86	1.01	0.28

Table 11
Temperature distribution obtained from ITT and FE model.

	Point A [°C]				Point B [°C]				Point C [°C]			
	ITT	SD ITT	FE	difference	ITT	SD ITT	FE	difference	ITT	SD ITT	FE	difference
Specimen 3	21.82	0.08	21.36	0.46	22.78	0.12	22.97	−0.19	20.05	0.32	19.58	0.47
Specimen 4	21.35	0.22	20.86	0.49	21.74	0.21	22.27	−0.53	21.30	0.30	20.28	1.02

Fig. 14. Temperature distribution for Specimen 3 with timber frame window.

Fig. 15. Temperature distribution for Specimen 4 with PVC frame window.

tion at a distance of 0.6 m from the left edge of the specimen. Point B is the location of a temperature peak at the edge of the window frame and at point C the temperature drops again at the window frame and polystyrene connection. For Specimen 3 with the timber frame window, excellent correlation is found between the ITT and FE temperatures at these three points shows good agreement with differences between the measured and simulated temperatures lower than 0.5 °C in all cases. For Specimen 4 with a PVC window, the temperatures provided by the ITT and derived from FE model for points A and B agreed to within ±0.5 °C while, for point C, a slightly higher difference of +1.0 °C was recorded. It can be noted from Figs. 14 and 15 that the zone of influence of the windows is greater in the ITT temperature profiles than for the FE predictions as was the case with the parallel thermal bridges. The differences in surface temperature distribution derived from the ITT and from the FE model are due in part to boundary conditions implemented in the FE model, as explained further in Section 5.1.1. Other reasons for the differences in surface distribution obtained from these two methods may be the assumed thermal properties input and the homogeneities of materials in the numerical analysis.

5.2.2. Comparison of window thermal bridging heat flow rate $\dot{Q}_{TB}$ and window thermal transmittance M-value

The thermal bridging heat flow rate $\dot{Q}_{TB}$ and thermal transmittance M-value of window specimens are presented in Table 12. In general, the results obtained from the ITT and from numerical simulations are in good agreement showing similar deviations from the hot box results. Considering $\dot{Q}_{TB}$ for Specimen 3, percentage deviations of +1.9% and −6.48% for the ITT and for FE model were recorded, respectively. For Specimen 4 both ITT and the FE model results show a deviation of about −8.0% compared to the $\dot{Q}_{TB}$ measured by the hot box. While considering the window thermal transmittance M-values for Specimen 3, the ITT value is within 0.61% and the FE value within −7.66% of the hot box measurements. For Specimen 4, the M-value measured by the ITT and simulated numerically deviates from the hot box measurement by about −9.5%. Considering the ITT results, a high level of accuracy with the hot box measurements was found for Specimen 3. For Specimen 4, the accuracy is less; however, as the error is less than 10%, it is a reasonable alternative to existing thermal bridging assessment methods. With regard to the FE results, their deviations from the hot box measurements may be explained by the assumed boundary conditions, thermal properties and the lack of accounting for workmanship mistakes and for material inhomogeneity, as previously mentioned in Section 5.1.2. An additional source of error could be the use of an area-averaged thermal conductivity for the PVC window frame in modeling Specimen 4. A sensitivity analy-

from both the ITT and the FE simulation are in excellent agreement with the TC measurements with a deviation of ± 0.30 °C for both methods. For point S2 on the polystyrene 'glazing', the temperature obtained from the ITT deviates by 1.20 °C for Specimen 3 and 1.00 °C for Specimen 4 from the TC measurements while the corresponding deviations for the FE model are 0.30 °C.

To facilitate discussion of the temperature disturbance at window frame and its connection to the wall unit and glazing, three points where peaks in the temperature distribution occur (Figs. 14 and 15) are considered. At point A, a temperature drop occurs as a result of thermal bridging at the wall and window frame connec-

Table 12
Window thermal bridging heat flow rate $\dot{Q}_{TB}$ and window thermal transmittance M-value.

		$\dot{Q}_{TB}$ and M results					Deviation from hot box [%]	
		hot box	u hot box	ITT	SD ITT	FE	ITT	FE
$\dot{Q}_{TB}$ [W]	Specimen 3	20.05	0.30	20.43	3.72	18.75	1.90	−6.48
	Specimen 4	20.66	0.30	19.00	0.38	18.93	−8.03	−8.37
M [W/K]	Specimen 3	0.691	0.011	0.695	0.118	0.638	0.61	−7.66
	Specimen 4	0.713	0.011	0.646	0.013	0.644	−9.35	−9.68

sis revealed that increasing thermal conductivity of this PVC frame by 20% results in a 2% higher thermal bridging heat flow rate. This demonstrates the significant influence of the thermal properties on the simulated $\dot{Q}_{TB}$ results.

6. Summary and conclusions

This paper has demonstrated the suitability of the indoor quantitative ITT for the heat loss assessment of multiple thermal bridges and windows in building components. A significant advantage of this methodology is that the actual heat loss associated with multiple thermal bridges and with windows installed into a building envelope can be determined without knowing the building envelope structure. As the actual heat loss is measured, factors that influence the thermal efficiency of a building such as interaction effects, material degradation over time or poor workmanship are automatically accounted for.

The developed methodology has been validated in the case of multiple parallel thermal bridges, such as occurs when steel columns form part of the building envelope. For these situations, the additional heat loss is expressed by thermal bridging heat losses q_{TB} and Ψ-values. Comparing the multiple thermal bridging heat losses q_{TB} and Ψ-values obtained from the ITT with those measured in calibrated hot box tests, the differences varied between -5.0% and $+2.5\%$ and between $+1.0\%$ and $+7.0\%$ for these two measures, respectively. The good agreement between these two measurements approaches points to the suitability of the proposed ITT method for parallel thermal bridging assessment. The distance between adjacent thermal bridges determines the degree of interaction between them; however, it was concluded that, when using the ITT methodology, it is not necessary to know the critical distance in advance. In the post-processing of IR images with two or more thermal bridges, the thermal bridge zone of influence of each thermal bridge is defined and the IR line is created. If the uniform surface temperature of the building envelope is not reached between the thermal bridges, it means they interact with each other. Therefore, the assessment of their heat loss should be evaluated from the same thermogram.

In the proposed methodology, the additional heat being dissipated because of the presence of a window is described by the thermal bridging heat flow rate $\dot{Q}_{TB}$. Using this measure, both the window thermal quality and the window installation, which may contribute significant additional heat loss, are assessed. A new window thermal transmittance or M-value is introduced, which is defined as the thermal bridging heat flow rate $\dot{Q}_{TB}$ per unit temperature difference between the indoor and outdoor environments. In tests on specimens containing timber- and PVC-framed windows, the $\dot{Q}_{TB}$ and M-values evaluated using the ITT deviated from the hot box measurements by between -8.0% and $+1.9\%$ and between -9.4% and $+0.6\%$. As the deviation in all measured cases are less than 10%, this suggests that this approach gives reasonable estimation of the actual thermal bridging performance.

The paper has demonstrated two different numerical approaches to multiple thermal bridges assessment, validated against the hot box measurements. These are FE steady-state heat transfer simulation and CFD analysis. The study revealed that time-consuming CFD modeling, where the convective air movements along the specimen were modelled explicitly, did not improve the results accuracy. The results show that the relatively more straight-forward FE heat transfer modeling approach is sufficient for predicting the thermal bridging heat losses. The thermography results were found to be in good agreement with the simulated results. It was possible to create these numerical models as the internal structure of tested specimens was known. However, in the case of existing buildings, this information may not be available, and so it is not possible to develop accurate numerical models. In these cases, in-situ measurement is the only way to evaluate thermal bridging performance. This study has shown that the indoor quantitative ITT can be applied in these cases.

The application of the indoor ITT methodology for evaluating heat loss through multiple parallel linear thermal bridges and through installed windows has been validated in laboratory conditions, using a hot box device. Testing the suitability of this method in the real conditions, on real buildings, under quasi-steady state conditions is required where some limitations and challenges are to be expected. The quasi-steady state needs to be maintained before and while performing the ITT survey. This may be challenging since outdoor conditions, such air temperature, solar radiation and wind, cannot be controlled. Some recommendations on choosing the optimum outdoor conditions can be found in Albatici at el. [47], who suggested that a deviation of up to 6 °C in the outdoor air temperature within 12 h before testing is acceptable. Solar radiation should be always avoided by carrying out the survey in the early morning before sunrise. With regard to the influence of wind, O'Grady at el. [22] showed how to adjust the Ψ-value obtained from ITT surveys carried out at different wind speeds to that at standard wind conditions. To achieve the recommended minimum difference of 10 °C [48] between the indoor and outdoor air temperatures for the ITT survey, it is often necessary to raise the indoor air temperature significantly. This can be created and controlled by the thermographer using a space heating system.

A practical application of this methodology would be for building thermal assessments before and after retrofitting of existing buildings, so that the actual improvement in thermal performance can be quantified. It could also be useful to building owners in planning their thermal retrofit strategy as priority could be given to those buildings where the need is greatest.

References

[1] International Energy Agency, Transition to Suitanable Buildings: Strategies and Opportunities to 2050, Paris 2013.

[2] Directive 2010/31/EU of the European Parliament and of the Council on the Energy Performance of Buildings 2010.

[3] European Commission, Evaluation of Directive 2010/31/EU on the energy performance of buildings, 2016.

[4] J. Goggins, P. Moran, A. Armstrong, M. Hajdukiewicz, Lifecycle environmental and economic performance of nearly zero energy buildings (NZEB) in Ireland, Energy Build. 116 (2016) 622–637.

[5] EN ISO 14683 Thermal Bridges in Buildings Construction – Linear Thermal Transmittance – Simlified Methods and Default Values, 2007.

[6] EN ISO 10211 Thermal Bridges in Building Construction – Heat Flow and Surface Temperatures – Detailed Calculations, 2017.

[7] A. Capozzoli, A. Gorrino, V. Corrado, A building thermal bridges sensitivity analysis, Appl. Energy 107 (2013) 229–243.

[8] H. Viot, A. Sempey, M. Pauly, L. Mora, Comparison of different methods for calculating thermal bridges: application to wood-frame buildings, Build. Environ. 93 (2015) 339–348.

[9] S. Hassid, Thermal bridges in homogeneous walls: a simplified approach, Build. Environ. 24 (1989) 259–264.

[10] S. Hassid, Thermal bridges across multilayer walls: an integral approach, Build. Environ. 25 (1990) 143–150.

[11] Building Regulation Conservation of Fuel and Energy Technical, Guidance Document Part L 2017.

[12] L. Zalewski, S. Lassue, D. Rousse, K. Boukhalfa, Experimental and numerical characterization of thermal bridges in prefabricated building walls, Energy Convers. Manag. 51 (2010) 2869–2877.

[13] F. Ascione, N. Bianco, R.F. De Masi, G.M. Mauro, M. Musto, G.P. Vanoli, Experimental validation of a numerical code by thin film heat flux sensors for the resolution of thermal bridges in dynamic conditions, Appl. Energy 124 (2014) 213–222.

[14] F. Ascione, N. Bianco, R. Francesca, D. Masi, F. De Rossi, G. Peter, Simplified state space representation for evaluating thermal bridges in building: modelling, application and validation of a methodology, Appl. Therm. Eng. 61 (2013) 344–354.

[15] H. Heinrich, K. Dahlem, Thermography of low energy buildings, In Proceedings of International Conference on Quantitative Infrared Thermography Qirt 2000, Reims, France.

[16] A. Wróbel, T. Kisilewicz, Detection of thermal bridges – aims, possibilities and conditions, In Proceedings of International Conference on Quantitative Infrared Thermography Qirt 2008, Cracow, Poland.

[17] M. Fox, S. Goodhew, P. De Wilde, Building defect detection: External versus internal thermography, Build. Environ. 105 (2016) 317–331.

[18] I. Benkő, Quantitative analysis of thermal bridges of structures through infrared thermograms, In Proceedings of International Conference on Quantitative Infrared Thermography Qirt 2002, Dubrovnik, Croatia, 203–208.

[19] F. Asdrubali, G. Baldinelli, F. Bianchi, A quantitative methodology to evaluate thermal bridges in buildings, Appl. Energy 97 (2012) 365–373.

[20] F. Bianchi, A. Pisello, G. Baldinelli, F. Asdrubali, Infrared thermography assessment of thermal bridges in building envelope: experimental validation in a test room setup, Sustainability 6 (2014) 7107–7120.

[21] M. O'Grady, A.A. Lechowska, A.M. Harte, Infrared thermography technique as an in-situ method of assessing the heat loss through thermal bridging, Energy Build. 135 (2017) 20–32.

[22] M. O'Grady, A.A. Lechowska, A.M. Harte, Quantification of heat losses through building envelope thermal bridges influenced by wind velocity using the outdoor infrared thermography technique, Appl. Energy 208 (2017) 1032–1052.

[23] T. Ward and C. Sanders, Conventions for Calculating Linear Thermal Transmittance and Temperature Factors, IHS BRE Press.

[24] ISO 10077-1:2006 Thermal performance of windows, doors and shutters – calculation of thermal transmittance – Part 1: general, 2017.

[25] ISO 12567-1 Thermal performance of windows and doors – determination of thermal transmittance by the hot-box method – Part 1: complete windows and doors, 2010.

[26] IP 1/06, Assessing the Effects of Thermal Bridging at Junctions and Around Openings, BRE Scotland, 2006.

[27] G.S. Wright, Calculating Window Performance Parameters for Passive House Energy Modeling, Passive House Institure US Tech Corner 1 (4) (2012).

[28] F. Cappelletti, A. Gasparella, P. Romagnoni, P. Baggio, Analysis of the influence of installation thermal bridges on windows performance: the case of clay block walls, Energy Build. 43 (2011) 1435–1442.

[29] EN ISO 8990 Thermal Insulation – Determination of Steady-State Thermal Transmission Properties – Calibrated and Guarded Hot Box, 1997.

[30] EN ISO 12412-2 Thermal Performance of Windows, Doors And Shutters – Determination of Thermal Transmittance by Hot Box Method – Part 2: Frames, 2003.

[31] Y. Fang, P.C. Eames, B. Norton, T.J. Hyde, Experimental validation of a numerical model for heat transfer in vacuum glazing, Sol. Energy 80 (2006) 564–577.

[32] F. Asdrubali, G. Baldinelli, Thermal transmittance measurements with the hot box method: calibration, experimental procedures, and uncertainty analyses of three different approaches, Energy Build. 43 (2011) 1618–1626.

[33] A.H. Elmahdy, Heat transmission and R-value of fenestration systems using IRC hot box – procedure and uncertainty analysis, Trans. ASHRAE 98 (1992) 630–637.

[34] M.J. Moran, H.N. Shapiro, B.R. Munson, D.P. Dewitt, Introduction to Thermal Systems Engineering: Thermodynamics, Fluid Mechanics and Heat Transfer, Hohn Wiley & Sons, Inc., 2003.

[35] ISO 18434-1 Condition Monitoring and Diagnostics of Machines – Thermography – Part 1: General procedure, 2008.

[36] Abaqus 6.13 User's manual, 2015.

[37] Product Data Sheet of Eurostrand OSB 3, E EGGER, 2009.

[38] http://hyperphysics.phy-astr.gsu.edu/hbase/Tables/thrcn.html#c1, thermal conductivity of steel, accessed on the 16.01.2017.

[39] Product Data Sheet of Styrofoam LBH-X, Dow Chemical Company Limited, 2014.

[40] https://www.engineeringtoolbox.com/thermal-conductivity-d_429.html, thermal conductivity of polyurethane foam, accessed on the 27.10.2017.

[41] www.engineeringtoolbox.com/metal-alloys-densities-d_50.html, density of steel, accessed on the 16.01.2017.

[42] https://www.engineeringtoolbox.com/density-materials-d_1652.html, density of polystyrene, accessed on the 27.10.2017.

[43] http://www.greenspec.co.uk/building-design/insulation-materials-thermal-properties/, density of polyurethane foam, accessed on the 27.10.2017.

[44] EN ISO 6946 Building Components and Building Elements – Thermal Resistance and Thermal Transmittance – Calculation Method, 2017.

[45] Ansys Fluent User's Manual, 2011.

[46] ISO/IEC Guide 98-3 Uncertainty of Measurement – Part 3: Guide to the Expression of Uncertainty in Measurement, 2008.

[47] R. Albatici, A.M. Tonelli, M. Chiogna, A comprehensive experimental approach for the validation of quantitative infrared thermography in the evaluation of building thermal transmittance, Appl. Energy 141 (2015) 218–228.

[48] Flir User's Manual for IR Cameras Flir Bxxx Series and Flir Txxx series, 2011.